

## NUMERICAL STUDY ON THE INFLUENCE OF WAKE CONTRACTION ON THE COMPUTATIONAL ACCURACY AND RAPIDITY OF A MODEL OF A ROTOR IN HOVER

Filip PANAYOTOV<sup>\*</sup>, Ivan DOBREV<sup>\*\*</sup>, Fawaz MASSOUH<sup>\*\*</sup>, Michael TODOROV<sup>\*</sup>

<sup>\*</sup>Technical University of Sofia, Bulgaria (michael.todorov@tu-sofia.bg)

<sup>\*\*</sup>Arts et Métiers - ParisTech, Paris, France (fawaz.massouh@ensam.eu)

DOI: 10.19062/2247-3173.2017.19.1.16

**Abstract:** *In the present article, the authors are performing a comparison study between two vortex models for the numerical computation of the static thrust of a model helicopter rotor in hover. The aim of this study is to access the rapidity and accuracy of the vortex models, comprised of a series of vortex rings and a single semi-infinite vortex cylinder. The first model has a cylindrical arrangement of the vortex elements, while the second model has a contracting arrangement of its vortex elements. Studies are performed for the optimal positioning and spacing of the vortex elements, in order to provide both rapid computation and good agreement with the experimental data, obtained from a wind tunnel test of the model rotor. The results of the study show a slight increase in the required computational time for the case of the contracting wake, while offering a significantly better accuracy than the cylindrical wake. Another interesting result from the numerical study is that in the case of the contracting wake model there is a reduction of the spacing (compression) between the vortex rings in the near wake, which results in the reduction of the overall length of the vortex system trailing downstream of the rotor.*

**Keywords:** *model rotor; hover; induced velocity; vortex ring; vortex cylinder; cylindrical wake; contracting wake,*

### 1. INTRODUCTION

The rotors of drones operate in unsteady operational conditions, as they are rarely performing long lasting hovers in zero wind conditions. Most of the time their utility is such that they are constantly maneuvering or performing thrust adjustments, in order to maintain stable flight or hover, while compensating for atmospheric disturbances. Thus of great interest is the rotor performance during transient or unsteady operational regimes.

The authors are aimed at the development of a numerical model, capable of rapid and accurate computation of the thrust of a hovering rotor. Such tool will allow the possibility to study the rotor performance in unsteady flow conditions, resulting from the transition from one operational regime to another or from phenomena, such as the tip vortex aperiodicity of a hovering rotor [1].

Nowadays, widespread is the use of CFD and BEM models for studies on UAV rotor performance and optimization of the blade geometry. Although their accuracy, the CFD models are computationally expensive and slow to perform when modeling the complete rotor geometry and the entire computational domain of the flow-field around it. This is due to the computation of Navier-Stokes equations for typically a few hundred-thousand up to a few million cells.

In [2] are summarized all major possibilities to speed up the computation with a CFD model, without losing any significant degree of accuracy. The most common solution is to couple the CFD simulation with other models, which allow for significant reduction of the required amount of numerical computations. In most cases, the CFD models are coupled with BEM or vortex models, which allow for the rapid determination of the aerodynamic loads on the blades or the induced velocity field around the rotor. This allows to save a significant amount of computational resources that contributes to the overall reduction of the computational time, although that the volume of required computations remains significant.

The BEM models can rapidly estimate the forces, acting on the blades of a rotor, as well as the radial distribution of the induced velocity. This allows for rapid evaluation of the overall rotor performance. However, the BEM models do not provide an insight for the flow-field outside the plane of the rotor.

Due to the aforementioned disadvantages of the CFD and BEM models, the authors chose to use the vortex theory for the development of a numerical model for the rapid computation of the thrust, produced by a rotor in transient or unsteady operational condition.

## 2. STATE OF THE ART OF HOVERING ROTOR MODELS

According to [3], Joukovsky performed a series of theoretical studies on propellers, which established the mathematical foundations for the vortex theory such as applied to rotors. Those works were followed by numerous flow visualization experimental studies on small scale and full scale helicopter rotors in both forward flight and hover. They added more clarity on the structure of the flow-field around a helicopter rotor. These studies also provided the first semi-empirical numerical models for hovering rotors, derived from the obtained experimental performance data and the geometry of the trailing wake.

Jenny et al. [4] and Landgrebe [5] proposed vortex models for the prediction of the hovering performance of helicopter rotors. These models consist of a helical wake, composed of helical vortex sheets, trailing from each one of the rotor blades. Simplifying assumptions are introduced, which allow the representation of the helical wake with a finite number of discrete vortex filaments, namely straight-line segmentation of the tip trailing helical vortex. The induced velocity field is computed with the use of the Biot-Savart law. These numerical models are capable to adequately predict the performance of a hovering rotor, although the simplifying assumption for a rigid helical wake introduces a significant error when the rotor is operating in too light or too heavy load conditions, corresponding to values of the coefficients of thrust  $C_T$  smaller than 0.0025 and bigger than 0.01. Another inconvenience is that for higher degree of accuracy a greater number of straight-line segments per complete helical turn must be considered and a greater number of complete helical turns must be taken into account, which significantly increases the volume of the required numerical computations.

Landgrebe [6], Miller et al. [7, 8] and Reddy [9] proposed an alternative approach for modeling the hovering rotor by decomposing the trailing wake into several parts, namely: near, intermediate and far. Each of those parts is modeled with a different type and amount of vortex elements with the aim to achieve greater accuracy, while offering significant numerical simplification. In the aforementioned papers demonstrated is the ability to obtain a significant degree of accuracy for the evaluation of the performance of hovering rotors with vortex systems, which comprise of less than 30 vortex elements in total.

Karpatne et al. [1] demonstrated the capabilities of a vortex model, in which the wake of the hovering rotor is modeled entirely with a system of vortex rings. In their model the vortex rings are emitted with a specific time-step, depending on the angular velocity of the rotor and are allowed to move freely under the induced velocities, resulting from the interaction with the remainder part of the previously emitted vortex rings. Reference [1] showed that the vortex models are capable to adequately simulate unsteady flow phenomena, thus allowing their study.

### 3. THE MILLER MODEL

Modeling the wake of a hovering rotor with a combination of different types of vortex elements for different segments of the wake is demonstrated in [1], [8] and [9]. The comparison study is performed with the vortex model proposed by Miller et al. in [8]. In the remainder part of the article it will be referred as the Miller model.

The wake of the Miller model consists of two parts: a near wake composed of 20 circular vortex rings arranged in series downstream of the rotor; and a far wake modeled by a single semi-infinite vortex cylinder, placed behind the last vortex ring of the near wake. Thus the model consists of only 21 vortex elements to be accounted for the computation of the entire flow-field around the rotor.

The semi-infinite vortex cylinder allows the model to compensate for the velocity deficit formed downstream of a wake when modeled with a series of vortex rings. It allows to stabilize the numerical computation and ensures that the induced velocities in the far wake double those induced in the rotor plane, such as per the theory for the hovering rotor.

Key for the degree of accuracy and the adequate operation of the model is the proper setup of the parameters  $d_0$ ,  $d_1$  and  $d_2$ , shown on Fig. 1.

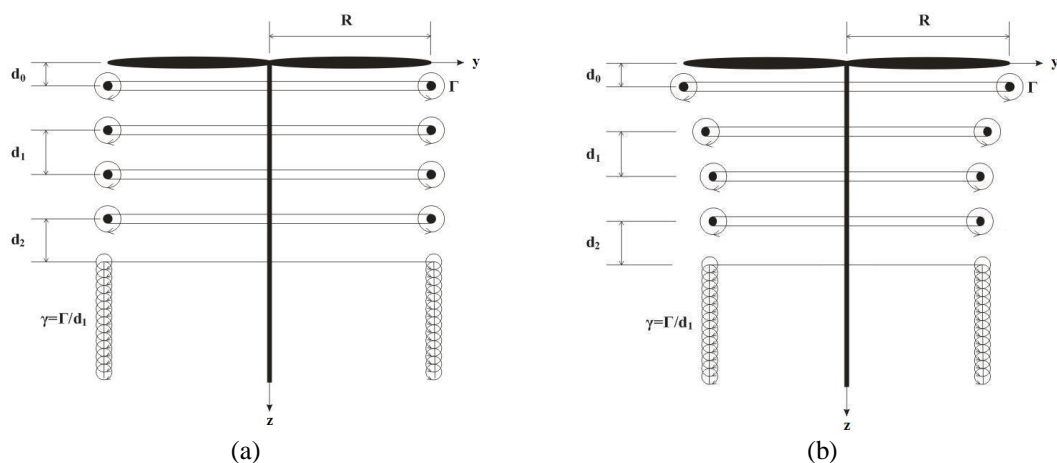


**FIG. 1.** The Miller model, composed of a series of vortex rings and a semi-infinite vortex cylinder. On Fig. 1 a) is presented the cylindrical arrangement of the vortex system. On Fig 1 b) is presented the initial prescribed position of the contracting wake, from which the computation is initialized.

The distance  $d_0$ , at which the first vortex ring is placed behind the rotor, has a key role for the distribution of the induced velocities along the blade. It is referred in [8] as the first blade-vortex encounter position, which represents the distance between the vortex ring emitted by the preceding blade and the following blade. This parameter can be varied, in order to study its influence on the induced velocity distribution on the blades and in the near wake downstream of the rotor.

The vortex rings are spaced between one another with  $d_1 = p/N_b$ , where  $p$  is the pitch of the helical wake, produced when the same operational conditions of the rotor are applied to the helical wake model and  $N_b$  is the number of the blades of the rotor. The distance  $d_2$  is the spacing between the last vortex ring of the near wake and the semi-infinite vortex cylinder, which models the far wake. The optimal values of the parameters  $d_0$  and  $d_2$  are estimated in a comparison between numerical and experimental data for multiple operational regimes of the rotor.

The Miller model offers the potential for rapid numerical computation when compared to CFD and BEM models due to the necessity to compute for significantly less amount of vortex elements. An additional reduction of the volume of numerical computations is possible for hover and vertical flight regimes due to the presence of axis-symmetric flow condition for the rotor. For the studied rotor with two blades, only half of the flow-field can be computed in order to visualize the entire flow around the rotor.

#### 4. NUMERICAL STUDIES

Performed are two numerical studies. The first one is aimed to find the optimal spacing parameters of the vortex elements in both wake models, namely:

- The best positioning of the initial vortex of the series of vortex rings  $d_0$ .
- The best positioning of the semi-infinite vortex cylinder after the last vortex ring of the near wake  $d_2$ .

The near wake is modeled with 20 vortex rings for both the cylindrical and the contracting arrangement of the vortex elements of the Miller model. The parameters  $d_0$  and  $d_2$  are varied as a percentage of the amplitude  $p$ , which represents the distance between two vortex rings, emitted by the same blade of the rotor.

The second numerical study compares the two vortex models with the aim to evaluate the accuracy and computational rapidity of the contracting wake model against the cylindrical wake model, thus benchmarking its performance capabilities. Studied is the distribution of the induced velocity along the blades of the model rotor for a specific set of operational regimes, namely for different combinations of angular velocity of the rotor  $\Omega$  and pitch angle of the blades  $\theta$ .

The results from the first study are presented in section 5 “Results from the numerical studies” sub-section 5.1 “Optimal parameter study”, while the results from the second study are presented in sub-section 5.2 “Comparison study”.

The model rotor, which is used as reference geometry in those studies, has two rectangular untwisted blades of NACA0012 profile. The tip radius  $R$  of the blades is 288mm, the root radius at the hub mounting  $r_0$  is 65mm and the chord length  $c$  is 25mm. The pitch angle of the blades is adjustable and thus can be varied between wind tunnel experiments.

Shown on Fig. 2 is the velocity triangle in a typical cross-section of the blade. The velocity of the axial flow through the plane of rotation of the rotor, resulting from the work of the rotor, is denoted with  $V_z$ . In the literature it is referred as the axial induced velocity and is a function of the operational parameters of the rotor, namely the angular velocity  $\Omega$  and the pitch angle of the blade  $\theta$ . The speed of rotation of the section in the plane of the rotor is denoted with  $U = \Omega y$ , where  $y$  is the blade station radius, which varies from  $r_0$  to  $R$ . For the tip of the blade  $y = R$  and  $U = \Omega R = V_{tip}$ . The relative air speed for the cross-section of the blade  $W$  is computed with (1):

$$W = \sqrt{U^2 + V_z^2} . \tag{1}$$

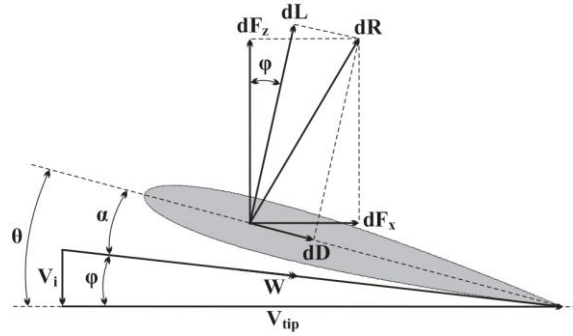


FIG. 2. Triangle of velocities in the cross-section of the rotor

#### 4.1 Assumptions

According to Miller et al. [8] for simplification purposes the wake may be considered as steady and its displacement can be limited in one of the three dimensions. Therefore, in order to reduce the numerical computations to a two-dimensional case, the following assumptions are taken:

- Hover flight is considered, thus the only axial velocity component, computed along the axis  $z$ , is the induced axial velocity  $V_z$  at that point.
- The wake is considered to be rigid, thus fixing a constant speed of displacement of the trailing vortices, equal to the induced velocity at the trailing edge of the blades [7, 8].
- The wake is steady, thus the induced velocity field of the rotor is independent from time.

These assumptions allow predetermining the exact positions of the trailing vortices, which technically is referred in the literature as a prescribed wake [7, 8].

#### 4.2 Numerical approach

According to [1], by assuming uniform bound circulation and a single tip-trailing vortex per blade, the vortex strength can be computed with:

$$\Gamma = \frac{2T}{\rho N_b R V_{tip}}, \quad (2)$$

where  $T$  is the total thrust produced by the model rotor at a fixed angular velocity  $\Omega$  and pitch angle of the blades  $\theta$ .  $R$  is the tip radius of the blades,  $V_{tip} = \Omega R$  is the velocity at the tip of the blades,  $N_b$  is the number of blades of the rotor and  $\rho$  is the density of the air.

For every change in either the angular velocity  $\Omega$  or the pitch angle of the blades  $\theta$ , the total thrust of the rotor  $T$  and the bound circulation  $\Gamma$  are also changed. Equation (2) is used for the computation of the bound circulation  $\Gamma$ .

In [13] the coefficient of thrust  $C_T$  is defined as:

$$C_T = \frac{T}{\rho A \Omega^2 R^2}, \quad (3)$$

where  $T$  is the total thrust produced by the rotor;  $\rho$  is the density of the air;  $\Omega$  is the angular velocity of the rotor;  $R$  is the radius of the rotor and  $A = \pi R^2$  is the area of the rotor disc. Equation (4) is used for the computation of the coefficient of thrust  $C_T$ .

From Fig. 2 it can be observed that for an increase of the axial induced velocity  $V_z$  there is a decrease of the angle of attack  $\alpha$ . The smaller is the angle of attack of the cross-sectional airfoil, the smaller is the local thrust increment  $\Delta F_z$ . Thus the total thrust of the rotor  $T$  reduces and with it reduces the coefficient of thrust  $C_T$ .

On Fig. 3 are shown the key dimensions, used in the computation of the induced velocity in a point of the flow-field. The dimensions  $y_m$ ,  $y_n$ ,  $z_m$  and  $z_n$  are universal for both the cylindrical and contracting wake models. Those are the coordinates of two points, namely M and N. It is considered that the induction happens in point M by a vortex element, situated at point N.

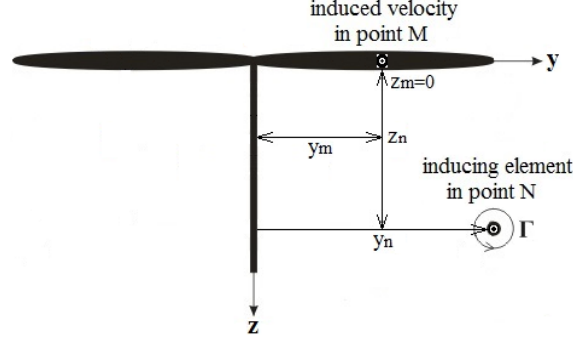


FIG. 3. Dimensions used in the computation of the induced velocity field of the rotor

Lewis [14] introduces the dimensionless parameters  $y$  and  $z$  with (4) and (5):

$$z = \frac{z_m - z_n}{y_n}, \quad (4)$$

$$y = \frac{y_m}{y_n}. \quad (5)$$

Those are used for the derivation of the equations for the axial  $V_z$  and radial  $V_y$  induced velocities. For the case of the semi-infinite vortex cylinder, the axial velocity is computed with (6) and for the case of  $y = 1$ , (7) is used:

$$V_{z,cyl} = \frac{\Gamma}{4\pi} \left\{ B + \frac{z}{\sqrt{z^2 + (y+1)^2}} \left[ K(k^2) - \frac{y-1}{y+1} \Pi(n, k^2) \right] \right\}, \quad (6)$$

$$V_{z,cyl(y=1)} = \Gamma \left( \frac{1}{4} + \frac{z K(k^2)}{2\pi\sqrt{z^2 + 4}} \right). \quad (7)$$

For the case of a semi-infinite vortex cylinder, the radial induced velocity is computed with (8):

$$V_{y,cyl} = \frac{2\Gamma}{\pi k^2 \sqrt{z^2 + (y+1)^2}} \left[ E(k^2) - \left( 1 - \frac{k^2}{2} \right) K(k^2) \right]. \quad (8)$$

The constant  $B$  in (6) depends from the ratio between the outer radius of the vortex cylinder and the radius of the rotor. For the case of  $y = 1$  it is:

$$B_{(y=1)} = \frac{\pi}{2}. \quad (9)$$

For the case of the system of vortex rings, the axial induced velocity is computed with (10) and for the radial induced velocity (11) is used:

$$V_{z,cyl} = \frac{\Gamma}{4\pi} \left\{ B + \frac{z}{\sqrt{z^2 + (y+1)^2}} \left[ K(k^2) - \frac{y-1}{y+1} \Pi(n, k^2) \right] \right\}, \quad (10)$$

$$V_{z,cyl(y=1)} = \Gamma \left( \frac{1}{4} + \frac{z K(k^2)}{2\pi\sqrt{z^2 + 4}} \right). \quad (11)$$

Equations (6), (7), (8), (10) and (11) contain complete elliptic integrals of the first  $E(k^2)$ , second  $K(k^2)$  and third order  $\Pi(n, k^2)$ . The elliptic parameters  $n$  and  $k$  are introduced with (12) and (13).

$$k = \sqrt{\frac{4y}{z^2 + (y+1)^2}}, \quad (12)$$

$$n = \frac{4y}{(y+1)^2}. \quad (13)$$

The amplitude  $p$  between two consecutive vortex rings, produced by the same blade is calculated with (14):

$$p = 2\pi R \tan(\varphi). \quad (14)$$

For a rotor with  $N_b$  number of blades the step between the vortex rings in the near wake  $d_l$  is calculated with (15):

$$d_l = \frac{p}{N_b}. \quad (15)$$

Equations (16) and (17) are introducing the initial contraction of the wake for the case of the Miller model with contracting arrangement of the vortex elements.

$$\frac{y}{R} = A + (1-A)e^{-ki2\pi}, \quad (16)$$

$$k = 0.145 + 27C_T. \quad (17)$$

The parameter  $A$  in (16) represents the ration between the radius of the flow-field in the far wake  $R_{fw}$  and the radius  $R$  of the hovering rotor. According to Leishman [13] most experimental studies confirm that  $A=0.78$  and not the theoretical value of 0.707.

For the Miller model the parameter  $i$  in (16) represents the number of the vortex elements that modify the trailing wake downstream of the rotor in hover.

The parameter  $k$  in (17) is introduced in order to modify the rate of contraction of the wake in function of the coefficient of thrust  $C_T$  of the hovering rotor. It is introduced for the first time by Landgrebe in [6]. In [9], Reddy uses the linear approximation for  $k$  such as proposed by Landgrebe, although that alternative non-linear equation do exist. However those alternative formulas for  $k$  are shown to give adequate results for a small range of values for  $C_T$ .

## 5. RESULTS FROM THE NUMERICAL STUDIES

### 5.1 Optimal parameters study

On Fig. 4 are shown six computational cases for the flow field of the model rotor in hover, computed with the Miller model. The numerical computations are performed for 2000 RPM and  $\theta=12\text{deg}$  for three different values of the parameter  $d_2$ , namely  $0.25p$  for case a) and d);  $0.5p$  for case b) and e); and  $0.75p$  for case c) and f). In all six cases  $d_0$  is set to  $0.1p$ . Situated in the left section of Fig. 4 are the computational cases a), b) and c), produced with the cylindrical wake model, while in the right section of Fig. 4 are situated computational cases d), e) and f), which are produced with the contracting wake model.

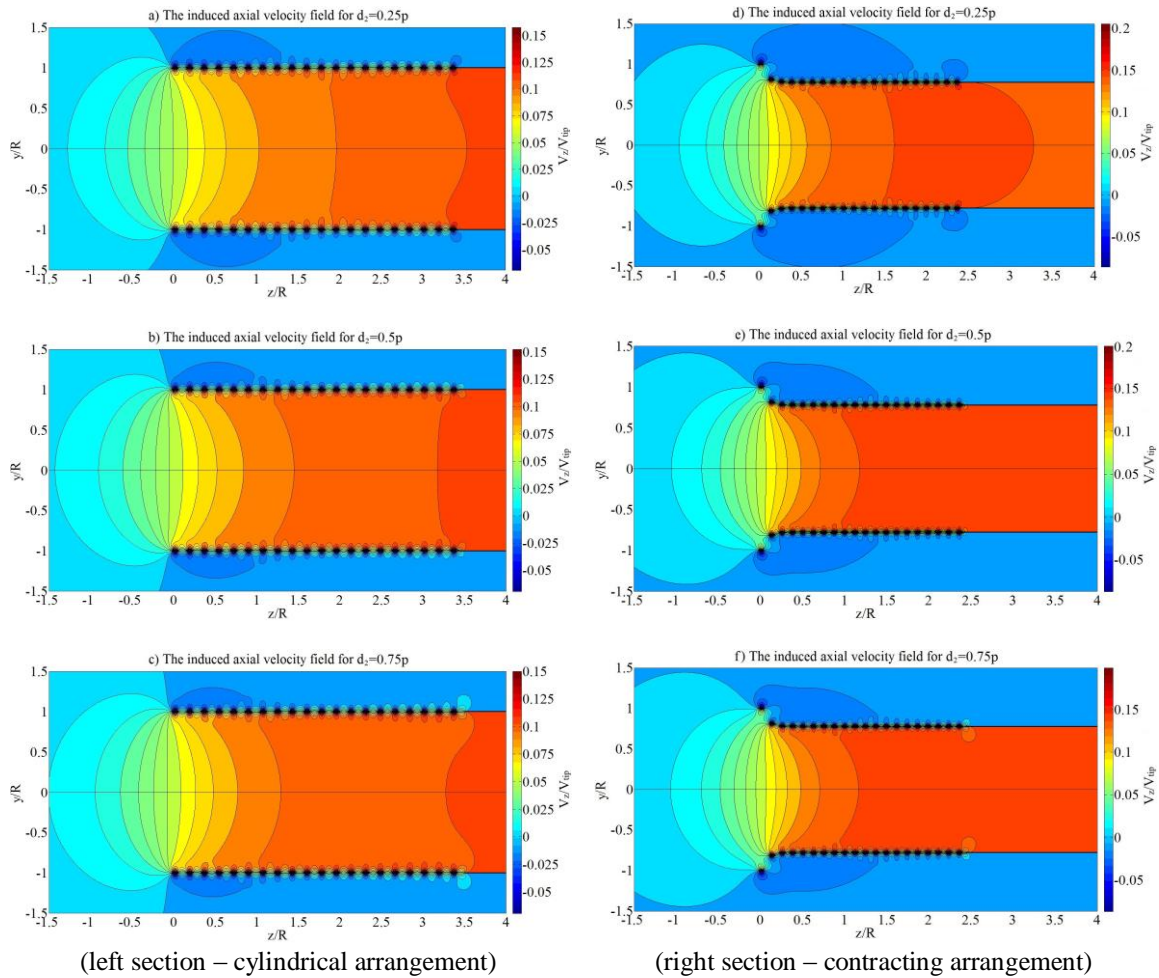


**FIG. 4.** The flow-field of the rotor computed with the Miller model for 2000 RPM and  $\theta=12\text{deg}$  for dimensions  $d_0=0.1p$  and  $d_2=\text{var}$ . On the left section of Fig. 4 are presented three computational cases for three value of  $d_2$  for the cylindrical arrangement of the vortex elements, while on the right section of Fig. 4 are presented the same three computational cases for the contracting arrangement.

On Fig. 5 a) is presented the optimal initial relative displacement  $d_0/R$  of the first vortex ring of the near wake of the rotor in function of the pitch angle of the blades  $\theta$ . On Fig. 5 b) is presented the optimal relative displacement  $d_1/R$  between the vortex rings in the near wake in function of the pitch angle of the blades  $\theta$ .

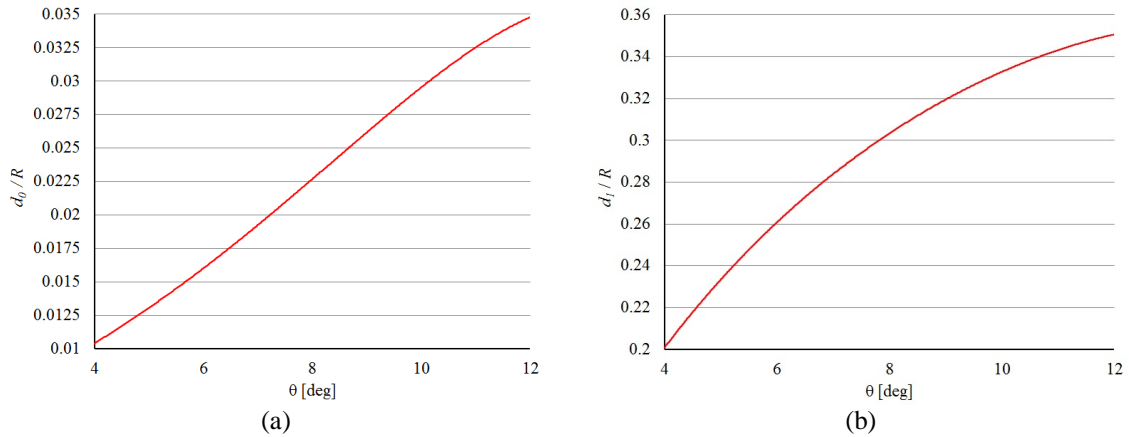


**FIG. 5.** The optimal values of the spacing parameters for the vortex system, non-dimensioned with the radius of the rotor  $R$ . On Fig. 5 a) is presented the function of the initial relative displacement of the first vortex ring  $d_0/R$  in function of the pitch angle of the blades of the rotor. On Fig. 5 b) is presented the relative spacing between the vortex rings  $d_1/R$  of the near wake in function of the pitch angle of the blades.

## 5.2 Comparison study

On Fig 6 a) is presented the relative axial induced velocity  $V_z/V_{tip}$ , computed with both models for 2000 RPM at blade-station  $y/R=0.75$  for pitch angle settings varying from 4 to 10 deg. The near wake is modeled with 20 vortex rings. The spacing parameters for both models are set to be  $d_0=0.1p$  and  $d_2=0.5p$ . The results from the numerical simulations are compared with the wind tunnel experimental data.

On Fig. 6 b) is presented the distribution of the relative induced axial velocity  $V_z/V_{tip}$  along the blade for the Miller model for 2000 RPM and  $\theta=10\text{deg}$  for both the cylindrical and the contracting wake. The near wake is modeled with 20 vortex rings. The spacing parameters for both models are set to be  $d_0=0.1p$  and  $d_2=0.5p$ .

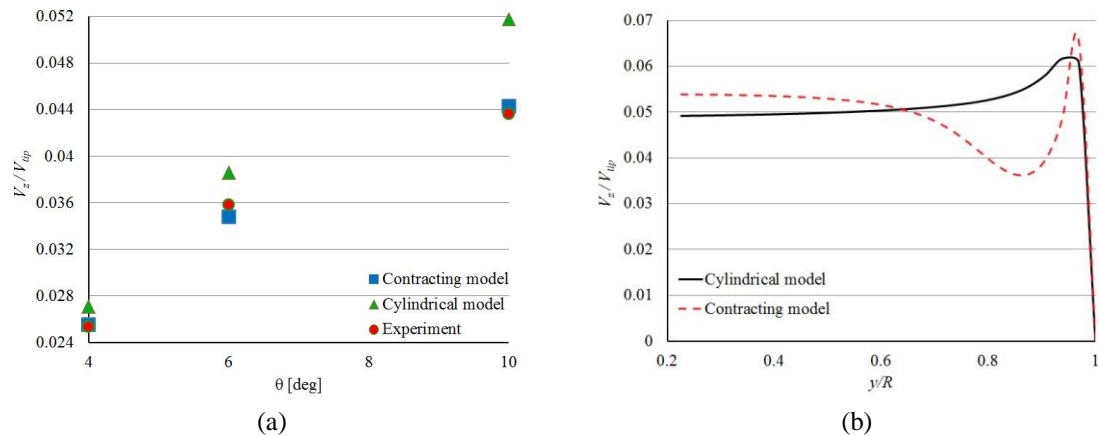


**FIG. 6.** The relative axial induced velocity  $V_z/V_{tip}$ . On Fig. 6 a) is presented the relative axial induced velocity  $V_z/V_{tip}$ , computed for 2000 RPM at blade-station  $y/R=0.75$ , in function of the pitch angle of the blades. On Fig. 6 b) is presented a comparison of the results for the relative axial induced velocity  $V_z/V_{tip}$ , computed along the blade for the cases of a cylindrical and contracting arrangement of the vortex elements.

In Table 1 are compared the relative axial induced velocity  $V_z/V_{tip}$  and the coefficient of thrust  $C_T$  for both arrangements of the vortex elements of the Miller model and the wind tunnel experiment for 2000 RPM and  $\theta=6\text{deg}$  at blade station  $y/R = 0.75$ . Presented are also the percentage error  $|\Delta|$  and the required computational time  $t_{comp}$  for both

simulations. The near wake is modeled with 20 vortex rings. The spacing parameters for both computations are set as follows:  $d_0=0.1p$  and  $d_2=0.5p$ .

Table 1. Comparison of the results obtained with both arrangement of the vortex elements of the Miller model, against the wind-tunnel experiment data

<b>Models</b>	<i>Cylindrical wake arrangement</i>	<i>Contracting wake arrangement</i>	<i>Wind tunnel experiment</i>
$V_z/V_{tip}$ [-]	0.03858	0.03479	0.03584
$C_T$ [ $10^{-3}$ ]	2.977	2.421	2.569
$ \Delta $ [%]	15.88	5.76	-
$t_{comp}$ [s]	0.18	0.22	-

## 6. DISCUSSIONS ON THE RESULTS

From the numerical results for the flow-field, presented on Fig. 4, it becomes apparent that the optimal value for the placement of the semi-infinite vortex cylinder behind the last vortex ring  $d_2$ , is the same as the spacing of the vortex rings in the near wake  $d_1$ . This is due to the fact that the most uniform velocity field is formed for  $d_2 = d_1$ , which can be observed on Fig. 4 b) for  $z/R = 3.3$  and on Fig. 4 e) for  $z/R = 2.5$ . It is also the only setting, for which the average computed value of the axial induced velocity  $V_z$  in the plane of the rotor  $z/R = 0$  double its value in the far wake beyond  $z/R = 5$ , such as predicted by the theory for a rotor in hover.

Such as shown on Fig. 5 a), the optimal value of the initial displacement of the first vortex ring  $d_0$  is found to vary approximately linearly with the pitch angle of the blades. Its value is approximately 1% of  $R$  for  $\theta=4\text{deg}$  and rises up to about 3.5% of  $R$  for  $\theta=12\text{deg}$ . The non-linear nature of the spacing between the vortex rings modeling the near wake is shown on Fig. 5 b).

From the results, presented on Fig. 6 a), it becomes apparent that the contracting wake model provides a better accuracy over the entire range of studied pitch angle settings. However, the accuracy of the numerical results, obtained with both wake models, depends significantly from the correct choice of the spacing parameters  $d_0$  and  $d_2$ . When the near wake is modeled with 20 vortex rings the average value of the required computational time for the cylindrical wake model is  $t_{comp} = 0.19$  s, while for the case of the contracting wake model  $t_{comp}$  increases slightly to 0.22 s.

From the results, presented on Fig. 6 b), it can be observed that the profile of the axial induced velocity distribution differs significantly between the two wake models. The contracting model induces slightly higher axial induced velocities inboard of the blade between sections  $y/R=0.2$  and  $0.6$ , followed by a slight drop around blade station  $y/R=0.8$  before rising again to form a peak toward the tip. In contrast, the cylindrical model induces an axial induced velocity distribution, which gradually increases from the root to the tip of the blade, while achieving a similar peak in both magnitude and position along the blade.

## CONCLUSION

The accuracy and rapidity of the numerical approach for the computation of the performance of a model rotor in hover was evaluated with two vortex based models.

Based on the results from the performed studies, it can be concluded that the Miller model with contracting arrangement of the vortex elements is only slightly slower than the cylindrical wake model in terms of computational speed, while providing significantly higher degree of accuracy.

The existing percentage error  $|\Delta|$  between the computational results and the experimental data for the axial induced velocity  $V_z$  is acceptable. Therefore, the contracting wake model can be used for preliminary studies and simulations of the expected thrust and overall performance of newly designed rotors.

## FUTURE WORK

The results from the conducted studies, presented in this paper, encouraged the authors to use the Miller model with the contracting arrangement of the vortex elements, in order to study the thrust of small UAV rotors in unsteady operational condition. The intent is to perform a series of studies on the rotor performance during transient operational regimes, produced by both big and small rates of change in the angular velocity of the rotor  $\Omega$ ; and for both positive and negative rates of change.

Of special interest is to study the changes in the thrust, resulting from a rapid change of the pitch angle of the blades  $\theta$  for a constant angular velocity of the rotor  $\Omega$ . Such a study will provide greater insights into the rotor performance during the transition period, in which the flow-field is adjusting to the new operational conditions of the rotor.

The future work on the model includes:

- To allow the numerical model to take into account the self-induced velocities of the vortex rings, which will in turn change the axial induced velocity  $V_z$  on the blade sections, thus redistributing the blade loads and affecting the bound circulation  $\Gamma$ .
- To allow the numerical model to dynamically change both the angular velocity of the rotor  $\Omega$  and the blade pitch angle  $\theta$ , thus allowing for the study of the dynamics of the rotor wake in the transition between different operational regimes of the rotor.
- To allow the possibility to vary dynamically  $d_0$  in function of the computed blade loading and the pitch angle of the blades of the rotor.
- To introduce the real fluid viscosity effects by taking into account the actual vortex core radius  $r_{vc}$ , which will vary in function of both the axial and radial displacements of the vortex elements in the free wake.

## REFERENCES

- [1] A. Karpatne, J. Sirohi, S. Mula and C. Tinney, "Vortex ring model of tip vortex aperiodicity in a hovering helicopter rotor", *Journal of Fluids Engineering, ASME*, vol. 136, 2014;
- [2] C. V. Velkova, *Modeling the Dynamic Behavior of Helicopter Rotors*, 2013-ENAM-0055, Paris, France, 2013;
- [3] V. I. Okulov, J. N. Soerensen and D. H. Wood, "The rotor theories by professor Joukowski: Vortex Theories", *Progress in Aerospace Sciences*, vol 73, 2015, pp. 19-46;
- [4] D. S. Jenney, J. R. Olson and A. J. Landgrebe, "A reassessment of rotor hovering performance prediction methods", *Journal of the American Helicopter Society*, Vol. 13, No. 2, April 1968, pp. 1-26;
- [5] A. J. Landgrebe, "An analytical and experimental investigation of helicopter rotor hover performance and wake geometry characteristics", *US Army Air Mobility Research and Development Laboratory, Technical Report 71-14*, Fort Eustis, Virginia, USA, June 1971;

- [6] A. J. Landgrebe, "An analytical method for predicting rotor wake geometry", *Journal of the American Helicopter Society*, Vol. 14, No. 4, October 1969, pp. 20-32;
- [7] R. H. Miller, "Rotor hovering performance using the method of fast free wake analysis", *Journal of Aircrafts*, vol. 20, 1983;
- [8] R. H. Miller, T. W. Roberts and E. M. Murman, "Computational methods for wake modeling and blade airload determination in hover and forward flight", *Computers and Mathematics with Applications*, vol. 12A, 1986;
- [9] K. R. Reddy, "The vortex flow-field generated by a hovering helicopter", 7th Australasian Hydraulics and Fluid Mechanics Conference, Brisbane, Australia, 18-22 August 1980;
- [10] J. Chattot and M. E. Braaten, "Wind turbine pitch change simulation with helicoidal vortex model", ASME, Turbo Expo 2012: Turbine Technical Conference and Exposition, Volume 6: Oil and Gas Applications; Concentrating Solar Power Plants; Steam Turbines; Wind Energy, pp. 789-796, June 2012, Copenhagen, Denmark, doi:10.1115/GT2012-68294;
- [11] S. Gupta and J. G. Leishman, "Accuracy of the induced velocity from helicoidal vortices using straight-line segmentation", *AIAA Journal*, Vol. 43, 2005;
- [12] W. Johnson, "Comparison of Calculated and Measured Model Rotor Loading and Wake Geometry", NASA, TM 81189, USA, 1980;
- [13] J. G. Leishman, *Principles of Helicopter Aerodynamics*, 1st ed., New York: Cambridge University Press, 2000, pp. 43-44;
- [14] R. I. Lewis, *Vortex Element Methods for Fluid Dynamic Analysis of Engineering Systems*. New York: Cambridge University Press, 1991, pp. 147-170.